Comparison of single and three-phase permanent magnet motor drives

Eduardo Santander, Hamid Ben Ahmed, Bernard Multon, Juliette Soulard, M. Rakotovao, Franck Barrere

Comparison of Single and Three-Phase Permanent Magnet Motor Drives

E. SANTANDER, A. BEN AHMED*, B. MULTON*, J. SOULARD
LESiR - URA CNRS D1375 - ENS de CACHAN - 61 av. du Pt. Wilson - 94235 CACHAN - FRANCE
* ENS Brittany Branch Campus de Ker Lann, 35170 Bruz

M. RAKOTOVAO, F.BARRERE
VALEO Systèmes d'Essuyage - 8 rue L. Lormand - 78321 LA VERRIERE - FRANCE

Abstract

This article presents a comparison between two PM synchronous electrical motors of 0.5kW, a single-phase machine and a three-phase machine designed for automotive applications. The single-phase structure developed by our laboratory displays the particularity of being completely symmetric: no mechanical or electromagnetic asymmetry. This machine starts with the maximum electromagnetic instantaneous torque and thus the corresponding current at the moment of start-up is very low. Both single- and three-phase motor drives are designed with the same specifications. The calculation and optimization of electromagnetic parts are obtained thanks to the use of a *corrected* 2D finite element code in order to take into account the strongly three-dimensional aspect of these machines. The experimental results and projection made using a 3D finite element code will serve to validate our method, which includes saturation problems. A simulation of electrical equations that correspond to the machine's operations is also developed and validated for each kind of motor inverter structure presented.

1 Introduction

Small electrical motors currently used in automotive industrial applications (wippers, cooling, starters, seat motors, etc.) are Brushed DC Motors because they offer the best solution for optimizing performance while maintaining a low cost price. However, the enhancement of both durability and the operating features required for such systems (safety, speed management, etc.) has led to the notion that brushless electrical motors could provide a good alternative for the future in this field. Since the cost is a very important factor in determining the feasibility of such a product (where the mechanical commutator is replaced by electronic switches and non-contact position sensors), the structures adopted for the study are single- and three-phase motor inverters. A single-phase structure has the advantage of requiring simplified control and power electronics compared to three-phase machines (lower number of transistors). Taking into account the fact that the cost of just one transistor is nearly that of a complete mechanical commutator, it is easy to understand why the electromagnetic optimization and the comparison of these two structures with respect to performance (efficiency, weight, switched currents, torque ripples, vibrations, etc.) are significant in selecting the best structure. The study presented in this paper concerns more precisely the calculation of an electrical motor-fan designed for the engine of automotive industry. In this application, the electrical motor is frequently located behind the radiator near the engine; ambiance conditions are consequently very hard (temperature, salt or other corrosive spray...). When vehicles are compact or if the place allowed near the engine is small, it is the case for air-conditioned vehicles, the electrical motor-fan axial length is of primary importance. In order to avoid contact between motor-fan and engine, it is necessary to get a compact electrical motor-fan structure. Figure 1 shows one solution of integration of the motor with the fan.

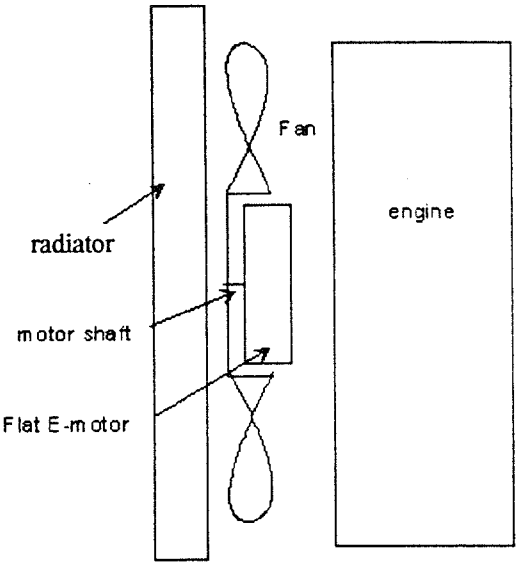

Figure 1: Flat electric motor-fan for engine cooling.

2 Electromagnetic Design Specificities

In order to reach the power required, as specifications impose a relatively small axial motor length, the motor's diameter must therefore be higher than its other dimensions (about 12 cm against 6 cm for the total axial length). Under these conditions, the motor has a « pancake » shape. The length of the motor's various component elements (along its axis of rotation) are very different from one another, as shown in Figure 2.
This configuration needs to be analyzed with a 3D finite element computation. Nonetheless it presents the drawback of requiring a sizable amount of both computing time and memory capacity. Such constraints prove burdensome when proceeding with the optimization of the machine's various geometrical parameters. The use of a 2D finite element code is better adapted to this kind of study. Yet, in our case, the

obtained computing accuracy is unacceptable if the input parameters have not been previously corrected with respect to the third dimension (axial).

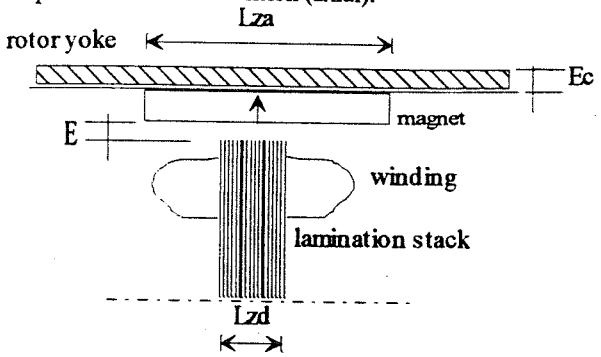

Figure 2: Diagram showing the 3D problem set-up.

In fact, the result of the flux computation is expressed per meter. Thus the problem must be modified in order to retain the same length reference (for example, that of the lamination stack). This is possible by defining both an equivalent remanent flux density (B_r) for the magnets and equivalent sections of yokes which allow the flux to cross. Concerning the first of these two requirements, the length difference is corrected by using the Carter coefficient which is introduced into the value of the magnetic remanent flux density, as proposed by F. Jean [1]. The reference length then corresponds to that of the lamination stack. The Carter coefficient expression is :

$$K_c = \left[1 - \left(\frac{L_{za}}{E} \right) . \frac{(1-s)^2}{5 + \left(\frac{L_{za}}{E} \right) . (1-s)} \right]^{-1} \qquad (1)$$

with $s = L_{zd} / L_{za}$. The remanent flux density of the magnets used for this calculation is thus:

$$B_{r_{equ}} = B_r . K_c \qquad (2)$$

Concerning the stator yoke thickness, preserving the area of the flux crossing leads to the definition of the equivalent thickness as follows:

$$E_{c_{equ}} = E_c \left(\frac{L_{zc}}{L_{zd}} \right) \qquad (3)$$

Under these conditions, we performed a non-linear calculation of the flux for different angular rotor positions on both the single- and three-phase first prototypes. Then, deriving this flux with respect to electrical angular rotor position, electromotive force (e.m.f.) of motors are obtained. The curves representing the e.m.f. as a function of mechanical angular position, which have been successfully compared with experimental results, are presented in Figures 3a and 3b.

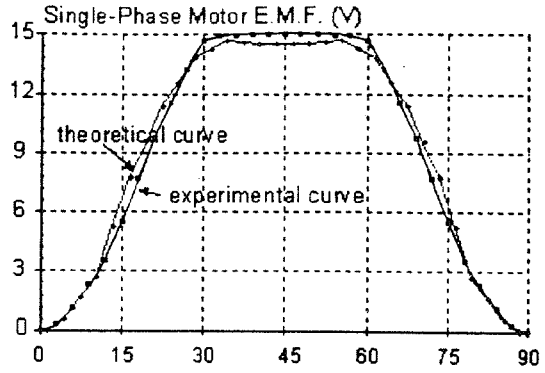

Figure 3a: Single-phase machine first-prototype e.m.f. (speed 2700rpm, e.m.f. vs. electrical degrees).

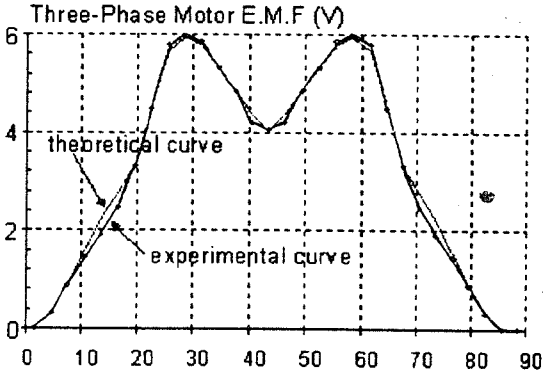

Figure 3b: Three-phase machine first-prototype e.m.f. (speed 2700rpm, e.m.f. vs. electrical degrees).

It shall be noted that saturation can be seen on these curves. It has already been noted for the first prototypes which have been calculated with a 2D finite element code without taking precisely into account the 3D effect mentioned above. Thanks to our approach, we could then modify the different yoke thickness and the drawing of laminations in order to avoid the saturation of both motors. The result of this 2D finite element simulation is illustrated in figures 4a and 4b which represent flux density lines in the single and three-phase motors for a rotor position where the flux is maximum through a winding or a phase.

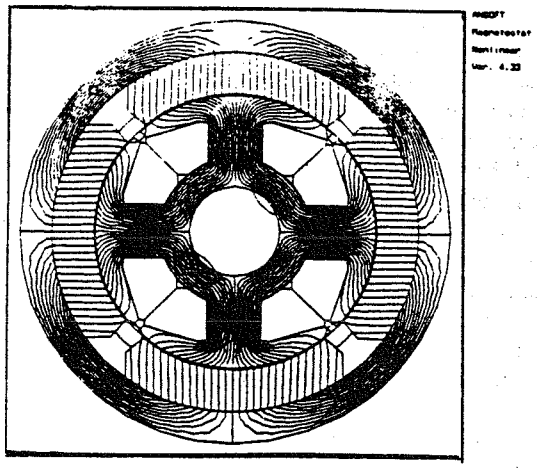

Figure 4a: Flux density lines inside the single-phase motor (corrected 2D model).

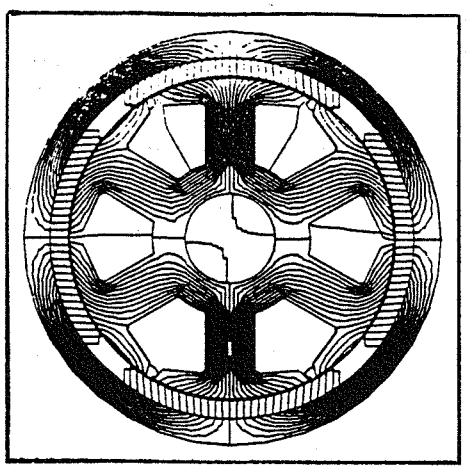

Figure 4b: Flux density lines inside the three-phase motor (corrected 2D model).

No saturation of motors allows to obtain e.m.f. wave-forms which are closer to a square signal in the case of the single machine and of a trapezoidal one for the three-phase motor as it is shown in figures 5 and 6. These curves have been obtained for the second prototypes.

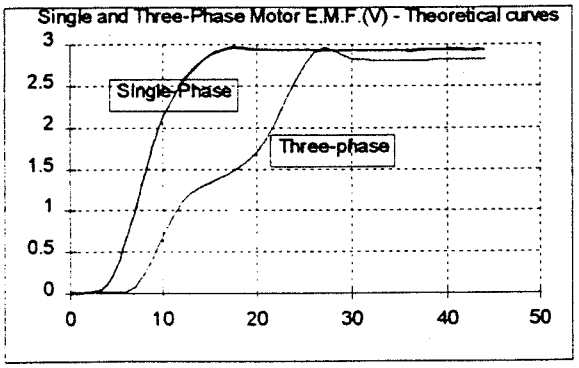

Figure 5: Single and three-phase motors e.m.f. per winding - Theoretical curves of second prototypes. (speed 2700 rpm, e.m.f. vs. electrical degrees).

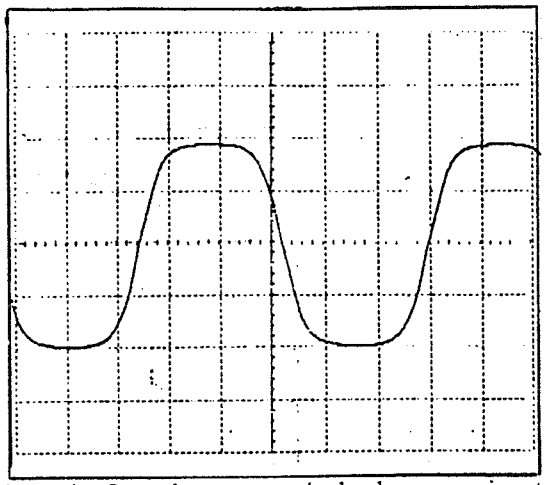

Figure 6a: Second prototype single-phase experimental E.M.F. (2700 rpm, 5 V/div - 2 ms/div).

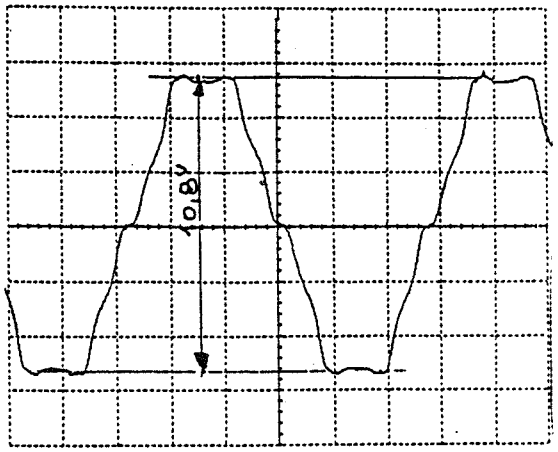

Figure 6b: Second prototype Three-phase experimental e.m.f. (2700 rpm, 2 V/div - 2 ms/div)

3 Single and Three-Phase Drives

Single and three-phase drives diagrams are presented in Figures 7a and 7b.

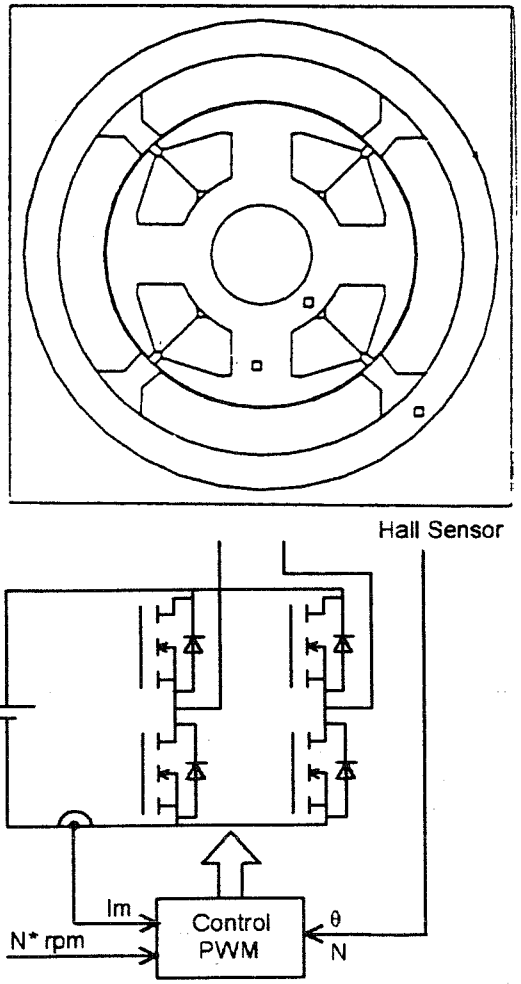

Figure 7a: Single-phase drive.

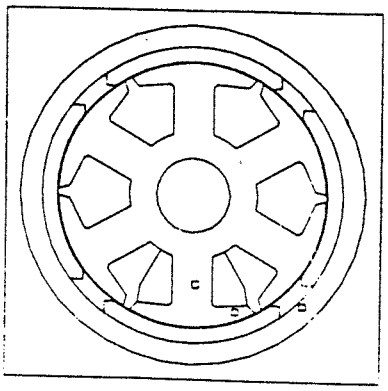

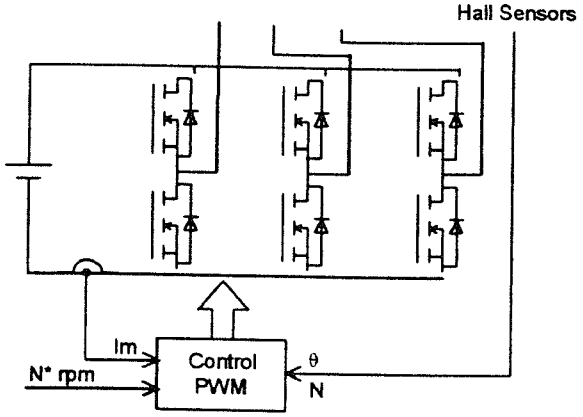

Figure 7b: Three-phase drive.

Hall effect sensors are to obtain the rotor position, one pulse per electric period in the case of the single drive and three pulses per electric period for the three-phase one.
Electrical motors are both four poles structures with salient armature poles and concentrated windings. Noting that single-phase structure has no dissymmetry but start up is obtained using an electromagnetic guile [3]. This solution does not affect the motor's performances.

Converters are full bridge (single phase) and three-phase bridge which allow the utilization of the maximum power per weight inside the volume ascribed to the motor. The comparison of performances is made using the same silicium area for the two converters which consist of both twelve Mosfet transistors (TO220 - Rds_{on}=10mΩ). Each of the four switches of the single-phase converter is composed of 3-parallel transistors while the three-phase converter (6 switches) uses 2-parallel transistors per switch only.
The improved electric motor speed control is obtained using a PWM current control. By varying the pulse width duty-cycle at a fixed frequency, the average current delivered by the DC supply is totally adjusted to get the speed reference. Transistor switch-instants define the electric angle δ between the e.m.f. and the voltage supply. This is mechanically fixed (position of the Hall sensor) in order to realize the maximum efficiency at high speed (100% duty cycle). In this case, the phase shift between current and e.m.f. is near to zero.

4 Performances

From the values of machine fluxes determined as a function of the rotor's angular position, the performances can be calculated thanks to a semi-analytical computation. The electrical equations are solved making reference to a supply circuit for just one winding comprising only one turn (see Figure 8). This allows writing just a single electrical equation [2] for the two motor structures, single- and three-phase :

$$u_n(\theta) = r_s.(ni) + P\omega.\frac{d(ni)}{d\theta} + \omega\frac{d\varphi_a(\theta)}{d\theta} \qquad (4)$$

with r_S the specific resistance and P the permeance.

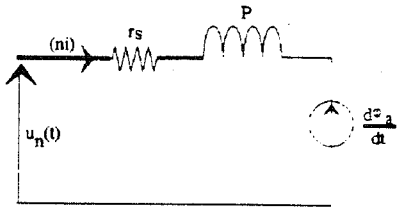

Figure 8: Equivalent electrical diagram for one turn per winding.

Using a Matlab environment, the current wave-form generated in the windings for a specific voltage supply is calculated. In order to determine the total current in the motor phase, the number of turns per winding is defined so that the drive efficiency is maximized. For this, an iterative computation is developed. The complete procedure of this method is summarised by the scheme presented in Figure 9 showing the different steps of the iterative computation.

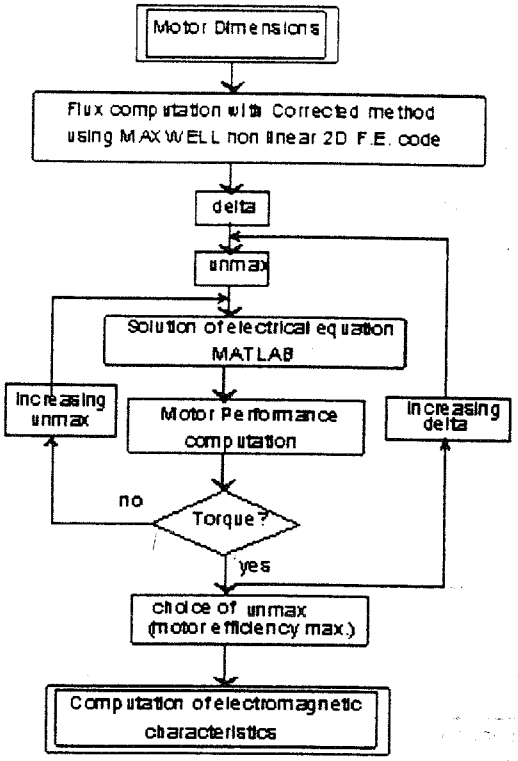

Figure 9 : Flow chart of the optimization of the motor performances.

For every value of the angle δ (equal to the angular shift between the e.m.f. $\left[\omega \frac{d\varphi_a}{d\theta}\right]$ and the imposed voltage supply), the maximum value $U_{n_{max}}$ of $u_n(\theta)$ which provides the average motor torque needed at the nominal speed is found. Then, the number of turns as a function of $U_{n_{max}}$ is calculated (see figure 10 where J_rms is also reported).

The evolution of motor and drive efficiencies are calculated too (see figure 11). The optimal number of turns is the one corresponding to a maximum drive efficiency. The calculation of overall motor performances is then made possible.

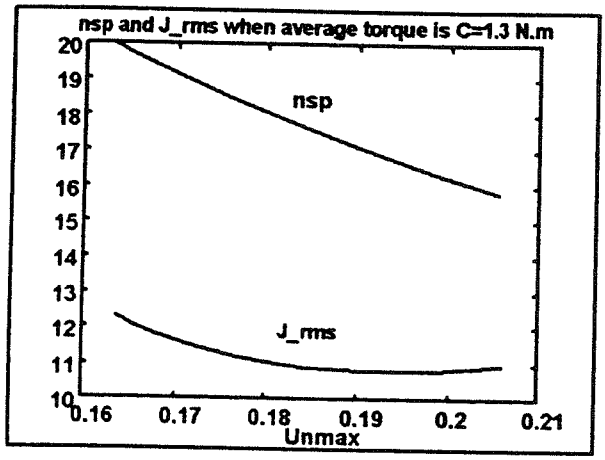

Figure 10 : Single-phase motor number of turns (nsp) and RMS current density (J_rms) as a function of Un_{max}.

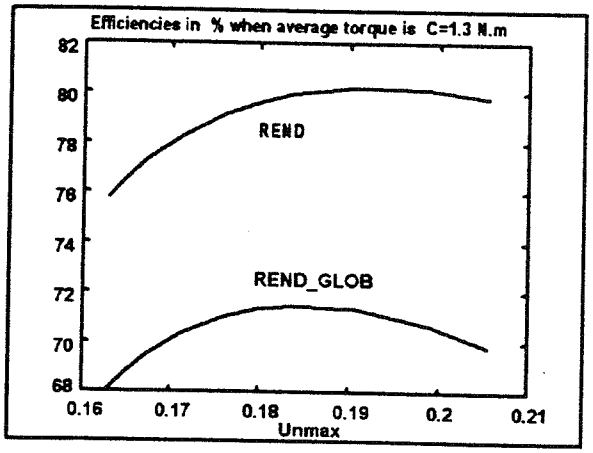

Figure 11 : Single-phase motor (REND) and drive (REND_GLOB) efficiencies as a function of Un_{max}.

The experimental electrical phase shift (δ) between the voltage supply and the single phase-motor e.m.f. which optimises the drive's performances at nominal speed is in concordance with theoretical prediction. The results are presented in the following Figure 12.

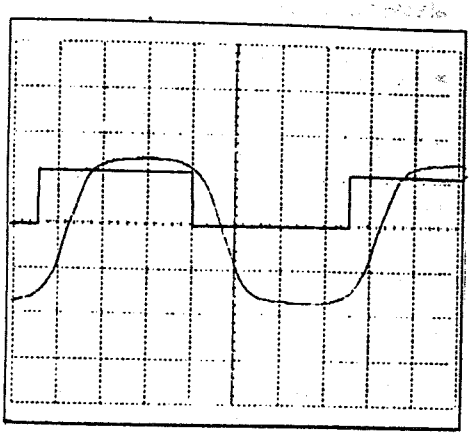

Figure 12 : Single-phase e.m.f. and Hall sensor signal (2 ms/div - 5 V/div).

5 Results and Comparison

Predicted current wave-forms for every motor phase have been compared to those obtained with prototypes designed using the method presented above. The comparison displays good agreement between theoretical and experimental curves as it is shown in figures 13 and 14 for the three-phase machine.

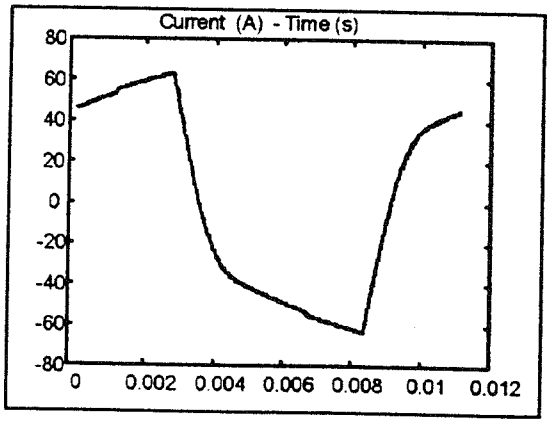

Figure 13a : Calculated current of the single-phase motor.

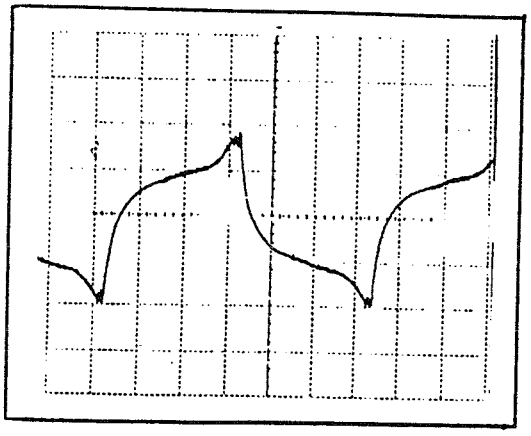

Figure 13b : Measured current of the single-phase motor (2 ms/div - 50 A/div)

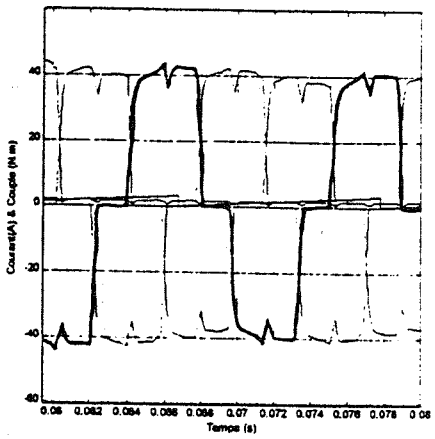

Figure 14a : Calculated current in one phase of the three-phase motor (2 ms/div - 20 A/div)).

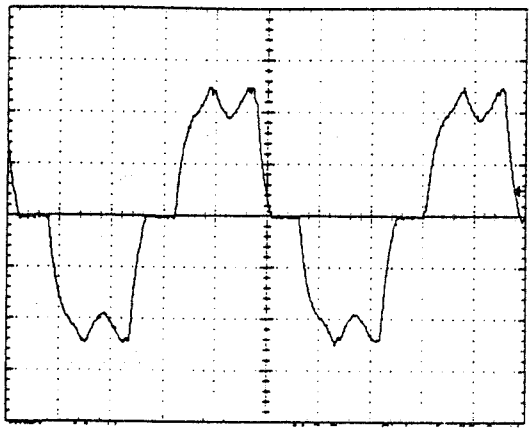

Figure 14b : Measured current in one phase of the three-phase motor (2.5 ms/div - 20 A/div).

Table 1 contains the results of this study. In Figures 15, the average current and efficiency drive were measured in operating conditions with the complete system (electric motor-fan in front of the radiator). It is shown that from the same set of specifications (torque, speed and motor volume), the performance of both single and three-phase motors are similar.

Type of drive	Three-phase	Single-phase
Total Joule losses (W)	62	90
Inverter losses (W)	60	80
Total absorbed power (W)	436	480
Overall efficiency (%)	70	64
Armature active mass (kg)	0.77	0.66
Inductor mass (kg)	0.55	0.70

Table 1: Comparison between the two motors using the same power silicium area and the same active part length. (C = 1.1 N.m, N = 2650 tr/min)

This comparison has been conducted with the same length of active motor parts, the same external diameter and the same power silicium surface for the inverter using MOS transistors. The transistor resistances Rdson of the three-phase bridge are thus 1.5 times greater than those of the single-phase inverter. However, it should be pointed out that although the active weight of the single-phase motor is 3 % higher than that of the three-phase motor, its efficiency is 6 points lower. This is probably due to a light saturation effect at high current.

6 Conclusion

In this article, a comparative study of two PM synchronous motor structures designed for applications in the automobile industry was presented. Part of this work consisted in the creation of 2D numerical taking into account the differences of length in the third dimension of our motors. The value of this method lies in providing engineers with a practical design and optimization tool which is easy to use, as opposed to 3D codes requiring an excessive amount of computing time and memory capacity. This approach has been combined with a semi-analytical computation that defines the number of turns to optimize the overall efficiency of the motor/converter assembly, on the basis of solving the electrical equation for one winding comprising just one turn. Model results have then been compared with experimental results. The agreement is quite good and validates our method (the difference is less than 5%). Moreover, a comparison between the two structures, single-phase and three-phase, reveals that it is quite possible to obtain comparable performances (the three-phase drive having slightly better ones) with the same specifications. Thus the choice of the structure will be made by considering other criteria such as : vibrations, torque ripples, cost, simplicity of the command, number of sensors, etc.... the last three examples of criteria being in favor of the single-phase drive.

References

[1] F. Jean, P. Brochet, C. Rombaut :"Taking account of some three-dimensional effects in the modeling of a Brushless Permanent-Magnet Motor". **IMAC'S** Electrimacs '96, Saint Nazaire, France, September 1996, pp. 639-644.

[2] B. Multon, M. Gabsi : "Influence de l'entrefer sur les performances et le dimensionnement d'un moteur à réluctance variable à double saillance et de sonorduleur". **7ème Congrès moteurs pas à pas, Nancy**, France, July 1992, pp. 34-50.

[3] E. Santander, A.Ben Ahmed, M. Gabsi : "Prediction of Cogging Torque of A Single Phase Machine". **Eight International Conference on Electrical Machines and Drives**, Cambridge, UK, 1-3 September 1997, EMD97, Conference Publication N°444, **IEE 1997**, pp. 210-214.

[4] J. Soulard : "Etude générale des limites de fonctionnement en régime de désexcitation avec prise en compte de la chute ohmique pour des moteurs synchrones à aimants permanents sans saillance". **JCGE'98**, Cachan, 27-29 avril 1998, pp 297-300.